Long Noncoding RNA lncSHGL Recruits hnRNPA1 to Suppress Hepatic Gluconeogenesis and Lipogenesis

Junpei Wang,[1,2] Weili Yang,[1,2] Zhenzhen Chen,[1] Ji Chen,[1] Yuhong Meng,[1] Biaoqi Feng,[1] Libo Sun,[3] Lin Dou,[4] Jian Li,[4] Qinghua Cui,[2] and Jichun Yang[1]

Diabetes 2018;67:581–593 | https://doi.org/10.2337/db17-0799

Mammalian genomes encode a huge number of long noncoding RNAs (lncRNAs) with unknown functions. This study determined the role and mechanism of a new lncRNA, lncRNA suppressor of hepatic gluconeogenesis and lipogenesis (lncSHGL), in regulating hepatic glucose/lipid metabolism. In the livers of obese mice and patients with nonalcoholic fatty liver disease, the expression levels of mouse lncSHGL and its human homologous lncRNA B4GALT1-AS1 were reduced. Hepatic lncSHGL restoration improved hyperglycemia, insulin resistance, and steatosis in obese diabetic mice, whereas hepatic lncSHGL inhibition promoted fasting hyperglycemia and lipid deposition in normal mice. lncSHGL overexpression increased Akt phosphorylation and repressed gluconeogenic and lipogenic gene expression in obese mouse livers, whereas lncSHGL inhibition exerted the opposite effects in normal mouse livers. Mechanistically, lncSHGL recruited heterogeneous nuclear ribonucleoprotein A1 (hnRNPA1) to enhance the translation efficiency of CALM mRNAs to increase calmodulin (CaM) protein level without affecting their transcription, leading to the activation of the phosphatidyl inositol 3-kinase (PI3K)/Akt pathway and repression of the mTOR/SREBP-1C pathway independent of insulin and calcium in hepatocytes. Hepatic hnRNPA1 overexpression also activated the CaM/Akt pathway and repressed the mTOR/SREBP-1C pathway to ameliorate hyperglycemia and steatosis in obese mice. In conclusion, lncSHGL is a novel insulin-independent suppressor of hepatic gluconeogenesis and lipogenesis. Activating the lncSHGL/hnRNPA1 axis represents a potential strategy for the treatment of type 2 diabetes and steatosis.

The human and other mammalian genomes produce a huge number of transcripts (1,2), 80–90% of which are not traditional protein-coding RNAs and termed long noncoding RNAs (lncRNAs) with the length >200 nucleotides (3–6). To date, a great number of lncRNAs have been identified in the tissues and circulation of humans and other mammals (6–10), and dysregulated lncRNA expression profiles are involved in the pathogenesis of many diseases (6,11–15). So far, the lncRNAs with function annotations are very few in number. Clearly, lncRNA is a huge treasure vault full of unknown but exciting molecules awaiting exploration.

There has been increasing evidence that lncRNAs regulate glucose and lipid metabolism. Dysregulated lncRNA expression profile is associated with islet dysfunction in humans (16). Knockdown of lncRNA TUG1 causes pancreatic β-cell dysfunction (17). lncRNA H19 regulates glucose metabolism by functioning as a sponge for microRNA let-7 (18,19). lncRNAs long noncoding liver-specific triglyceride regulator (lncLSTR) and MEG3 also regulate hepatic glucose and lipid metabolism (20,21). On one hand, the effects and mechanisms of the reported lncRNAs in glucose and lipid metabolism in various tissues need further validation (16,18–21). On the other hand, to further characterize new lncRNAs that regulate glucose and lipid metabolism is also of great importance. Particularly, identifying new

[1]Department of Physiology and Pathophysiology, School of Basic Medical Sciences, Key Laboratory of Molecular Cardiovascular Sciences of the Ministry of Education, Center for Non-coding RNA Medicine, Peking University Health Science Center, Beijing, China
[2]Department of Biomedical Informatics, School of Basic Medical Sciences, Key Laboratory of Molecular Cardiovascular Sciences of the Ministry of Education, Center for Non-coding RNA Medicine, Peking University Health Science Center, Beijing, China
[3]Beijing You An Hospital, Capital Medical University, Beijing, China
[4]Key Laboratory of Geriatrics, Beijing Institute of Geriatrics & Beijing Hospital, Ministry of Health, Beijing, China

Corresponding author: Jichun Yang, yangj@bjmu.edu.cn, or Qinghua Cui, cuiqinghua@bjmu.edu.cn.

Received 9 July 2017 and accepted 16 January 2018.

This article contains Supplementary Data online at http://diabetes.diabetesjournals.org/lookup/suppl/doi:10.2337/db17-0799/-/DC1.

J.W. and W.Y. contributed equally to this work.

lncRNAs that regulate hepatic gluconeogenesis will shed light on the pathogenesis of type 2 diabetes.

A great number of new lncRNAs were identified in mouse liver and plasma in our previous studies (7,8). Eleven lncRNAs dysregulated in liver after ischemia/reperfusion injury (IRI) had been validated and identified with high expression (7,8). Among these 11 lncRNAs, AK143693 is a nonsecretory lncRNA that exhibits high expression in mouse liver with unknown function(s) (7,8). We found in the preliminary experiment that AK143693 silencing increased lipid deposition in liver after IRI (Supplementary Fig. 1*A* and *B*), suggesting it may play roles in regulating hepatic glucose/lipid metabolism. The current study revealed that lncRNA AK143693 functions as a novel suppressor of hepatic gluconeogenesis and lipogenesis (SHGL) and is renamed as lncSHGL.

lncSHGL expression was reduced in obese mouse livers. lncRNA B4GALT1-AS1, the human homologous sequence of mouse lncSHGL, was also reduced in human livers with steatosis. Hepatic lncSHGL overexpression suppressed gluconeogenesis and attenuated hyperglycemia and fatty liver in mice fed a high-fat diet (HFD), whereas hepatic lncSHGL repression promoted hyperglycemia and lipid deposition in normal mice. Mechanistically, lncSHGL recruited heterogeneous nuclear ribonucleoprotein A1 (hnRNPA1) to enhance calmodulin (CaM) mRNAs translation. An increase in the CaM protein level finally suppressed gluconeogenic and lipogenic pathways in an insulin- and calcium-independent manner in hepatocytes.

RESEARCH DESIGN AND METHODS

Experimental Animals

Male C57BL/6 mice (8 to 10 weeks old) were fed a 45% HFD for 3 months to induce diabetic and steatotic phenotypes (22,23). The study also used 10- to 16-week-old male *db/db* mice on a BKS background. All animal experimental protocols complied with the Animal Management Rules of the Ministry of Health of the People's Republic of China and the Peking University Guide for the Care and Use of the Laboratory Animals.

Antibodies

Anti-phosphorylated (p)Akt (phosphorylation at Ser473 site) and Akt antibodies were purchased from CST. Other antibodies were obtained from Santa Cruz Biotechnology, CST, or other commercial companies.

Adenoviral Overexpression of lncSHGL in HFD Mouse Livers

An adenovirus (Ad) expressing lncSHGL was constructed according to the AK143693 sequence in the PubMed database (https://www.ncbi.nlm.nih.gov/nuccore/AK143693) (7,8). To overexpress lncSHGL in mouse livers, 1.0×10^9 plaque forming units Ad-lncSHGL or Ad-green fluorescent protein (GFP) were injected into mice via tail vein. Oral glucose tolerance tests (OGTTs), insulin tolerance tests (ITTs), and pyruvate tolerance tests were performed at the 7th day after viral injection using different sets of mice. On the 9th day, the mice were sacrificed on fed state. The serum and tissues were collected for biochemical analyses.

Knockdown of lncSHGL in C57BL/6 Mouse Livers

Stealth small interfering (si)-lncSHGL were synthesized by Invitrogen (sequences provided in Supplementary Table 1). The siRNA mixture was injected into C57BL/6 mice via tail vein (2.5 mg/kg body weight in 100 μL sterile saline) (23,24), the same dose of scrambled siRNA (Invitrogen) was used as the control. OGTTs were performed 72 h after the siRNA injection. On the 4th day, the mice were sacrificed for experimental analyses.

Cell Culture

Cell lines or primary mouse hepatocytes were infected with 50 multiplicity of infection of Ad-lncSHGL or Ad-GFP for 24 h. For insulin-stimulation experiments, infected cells were serum starved for 12 h, followed by treating with 100 nmol/L insulin for 5 min. For inhibition of phosphatidyl inositol 3-kinase (PI3K) or P2 receptors or calcium signaling, infected cells were treated with 1 μmol/L wortmannin, 50 μmol/L pyridoxalphosphate-6-azophenyl-2',4'-disulfonic acid, 50 μmol/L suramin, 100 μmol/L chlorpromazine (CPZ), an inhibitor of CaM (25), 10 μmol/L nifedipine, or 10 μmol/L 2-aminoethoxydiphenyl borate for 1 h before experimental assays. For depleting extracellular Ca^{2+}, infected cells were treated with Ca^{2+}-free medium plus 0.5 mmol/L EGTA for 2 h, and chlorpromazine was added 1 h before experimental assays.

Plasmid Overexpression of Genes in Hepatocytes

Cells plated in six-well plates were transfected with 5 μg plasmid for 24 h. Plasmids expressing human *CALM1-2* and *hnRNPA1* plasmids were purchased from OriGene (CALM1, Cat No. SC115829) and Vigene Biosciences China (CALM2, Cat No, CH809926; hnRNPA1, Cat No CH877838), respectively.

Determination of Gene Expression at mRNA and Protein Levels

Target gene mRNA level was normalized to that of β-actin in real-time PCR assays. Each sample was assayed in duplicate in each experiment. All primer sequences are provided in Supplementary Table 2. The protein levels were analyzed by immunoblotting assay. For protein blot quantitation, each protein (nonphosphorylated) was first normalized to the corresponding housekeeping protein β-actin, and then the value was normalized to the control value in each experiment. For quantitation of phosphorylated protein, phosphorylated protein was first normalized to the corresponding total protein and then was normalized to the control value.

Cellular Calcium Determination

Cells seeded on coverslips were loaded with 1 μmol/L Fura-2 acetoxymethyl ester for 30 min, followed by Ca^{2+} level determination under Olympus IX71 fluorescence microscope. The emission intensities at the wavelengths of 340 nm and 380 nm were recorded every 1 s, and the average ratio

of the emission densities (F340-to-F380) in 300 s reflected the basal free calcium level (22,23).

Confocal Analysis of FOXO1 Distribution

Cells seeded on coverslips were infected with Ad-lncSHGL for 24 h. The coverslips were blocked in 1% BSA for 30 min at 37°C after washing with PBS. The coverslips were incubated with anti-FOXO1 antibodies at 4°C overnight, and washed with PBS, followed by detection with goat anti-rabbit Alexa Fluor 594. After nuclear staining with DAPI, coverslips were mounted on glass slides using 50% glycerol in PBS. Imaged were visualized by fluorescence microscopy using a confocal laser scanning microscope.

Glucose Production Assay

As detailed previously (26), cells were infected with Ad-lncSHGL for 24 h and then treated with DMEM/high-glucose medium containing 20 mmol/L sodium lactate/2 mmol/L sodium pyruvate without glucose or phenol red (Gibco) for another 16 h, followed by treatment with 10 nmol/L insulin for 3 h. The culture medium was centrifuged to collect the supernatant for analyzing glucose content with the Glucose Assay Kit (Sigma-Aldrich). The glucose data were normalized with the cellular protein content (micrograms per milligram of protein).

DNA-RNA Pull-Down Assay

PCR products labeled with or without biotin were amplified by PCR (each PCR product position in lncSHGL is provided in Supplementary Table 2) and purified. National Collection of Type Cultures (NCTC)-1469 cells infected with Ad-lncSHGL were cross-linked by ultraviolet exposure (400 mJ/cm^2). Cells were lysed in RNA immunoprecipitation (RIP) buffer (20) and centrifuged at 12,000 rpm for 10 min to collect the supernatant. Purified PCR products (1–2 μg) were added into 1 mg supernatant protein after shortly heating at 95°C, and then quickly cooled on ice. The mixture of DNA and protein was incubated at 37°C for 4 h. Washed Dynabeads M-280 streptavidin (80 μL; Invitrogen) were added to each sample and incubated at room temperature for 30 min. Beads were washed five times with binding and washing buffer, and then boiled in 1×SDS loading buffer for 5 min. The samples were separated by PAGE and then subjected to silver staining and Western blotting assays. The target protein bands were analyzed by mass spectrometry (MS).

RIP

The method for RIP was described previously (27). Anti-hnRNPA1 antibody or rabbit IgG (4 μg) was added to 40 μL Protein A Resin (TransGen Biotech) with 100 μL coupling buffer (Thermo Scientific), and the mixture was incubated at 4°C for 1 h with gentle rotation. Cells treated with Ad-lncSHGL were crosslinked by ultraviolet exposure. Cells were lysed and centrifuged at 12,000 rpm for 10 min to collect the supernatant. Supernatant protein (1 mg) was added into each binding reaction and incubated at 4°C overnight. The Protein A Resin/protein mixture was washed with RIP buffer and resuspended in 500 μL Trizol for RNA extraction. The isolated RNAs were detected by real-time PCR with the normalization to control value.

Lipolysis of Adipose Tissue

Epididymal adipose tissue (50 mg) was dissected from mice and suspended in 500 μL phenol red-free DMEM (fDMEM) containing 5 mmol/L glucose, and horseradish peroxidase–conjugated IgG on ice and cut into 1 mm^3 pieces. The samples were incubated at 37°C in 5% CO_2-95% air in 500 μL fDMEM for 30 min, washed three times, and incubated in 500 μL fDMEM. The medium was collected at 30 and 120 min for glycerol release measurement (28). The glycerol level was normalized with protein content.

Ribosome Extraction

The protocol for ribosome extraction was detailed previously (29). Treated cells were lysed in 0.5 mL radioimmunoprecipitation assay buffer (BioTeke Corporation). After being incubated 30 min on ice, the samples were centrifuged at 12,000 rpm at 4°C for 10 min to collect the supernatant. The supernatant was added to 9.5 mL precooled 30% sucrose buffer (20 mmol/L HEPES [pH 7.4], 50 mmol/L potassium acetate, and 5 mmol/L magnesium acetate; 1 mmol/L dithiothreitol, protease inhibitor cocktail, and recombinant RNase inhibitor were added before using), and centrifuged at 30,000 rpm at 4°C for 2 h. The pellets were resuspended in 1 mL precooled Buffer A (10 mmol/L HEPES [pH 7.9], 10 mmol/L KCl, 1.5 mmol/L $MgCl_2$, 0.3 mol/L NaCl, and recombinant RNase inhibitor were added before using). After being incubated on ice for 1 h, the samples were centrifuged at 10,000 rpm at 4°C for 15 min to collect the supernatant for RNA determination. The same amount of RNAs was analyzed by real-time PCR with the data normalized to control values.

Hydrodynamics-Based Plasmid Overexpression of hnRNPA1 or CaM in C57BL/6 Mouse Livers

Hydrodynamics-based transfection in animals by tail vein administration of naked plasmid DNA was detailed previously (30–32). Briefly, HFD mice were divided into three groups based on OGTT. Endotoxin-free plasmid (50 μg) was dissolved in sterile saline with the volume of 8% of the body weight at room temperature and injected into tail vein in 7 s. OGTTs were performed 72 h after the plasmid injection. Mice were sacrificed 24 h later for assays, as described above.

Human Liver Samples

Six steatotic and healthy liver samples were selected from 11 pairs of liver samples in the previous study (33). The ethics issue and biochemical characteristics of these six pairs of steatotic patients and healthy subjects were described previously (28,33).

Statistical Analysis

Data are presented as the mean ± SEM. Statistical significance of differences between groups was analyzed

by the *t* test. *P* values <0.05 were considered statistically significant.

RESULTS

lncSHGL Expression Was Reduced in Obese Mouse Livers

Mouse lncSHGL is located in chromosome 17 between protein-coding sodium/calcium exchanger one isoform ×5 and extracellular tyrosine-protein kinase PKDCC precursor genes (Supplementary Fig. 1*A*) (7,8). In the preliminary study, we found that lncSHGL inhibition increased lipid deposition in the liver after IRI (Supplementary Fig. 1*B*). There is no open read frame >200 base pairs (66 aa) in the lncSHGL sequence (data not shown). lncSHGL is highly expressed in mouse metabolic tissues (Supplementary Fig. 1*C*). lncSHGL and AK139328 were reduced, whereas the other nine lncRNAs remained unchanged in HFD mouse livers (Fig. 1*A*). lncSHGL, AK139328, AK143294, and ENSMUST00000151138 were reduced, AK054386 was increased, and the other six lncRNAs were not changed in *db*/*db* mouse livers (Fig. 1*B*). In contrast, lncSHGL expression remained unchanged in muscle, heart, pancreas, and adipose tissues of obese diabetic mice (Supplementary Fig. 1*D* and *E*). Time-course analyses of HFD feeding on hepatic lncSHGL expression revealed that it was increased at 1 and 2 months but was decreased at 3 months after HFD feeding (Supplementary Fig. 2*A*). In NCTC-1469 cells (normal mouse liver cell line), free fatty acids (FFAs) increased lncSHGL expression at 6 h of treatment but repressed it after 18 h of treatment. Glucose similarly repressed lncSHGL expression after 18 h of treatment (Supplementary Fig. 2*B* and *C*). lncRNAs generally exhibit low sequence conservation across species. We had searched human homologous sequences of lncSHGL using National Center for Biotechnology Information Basic Local Alignment Search Tool (BLAST). As a result, the noncoding RNA B4GALT1-AS1 (34), whose

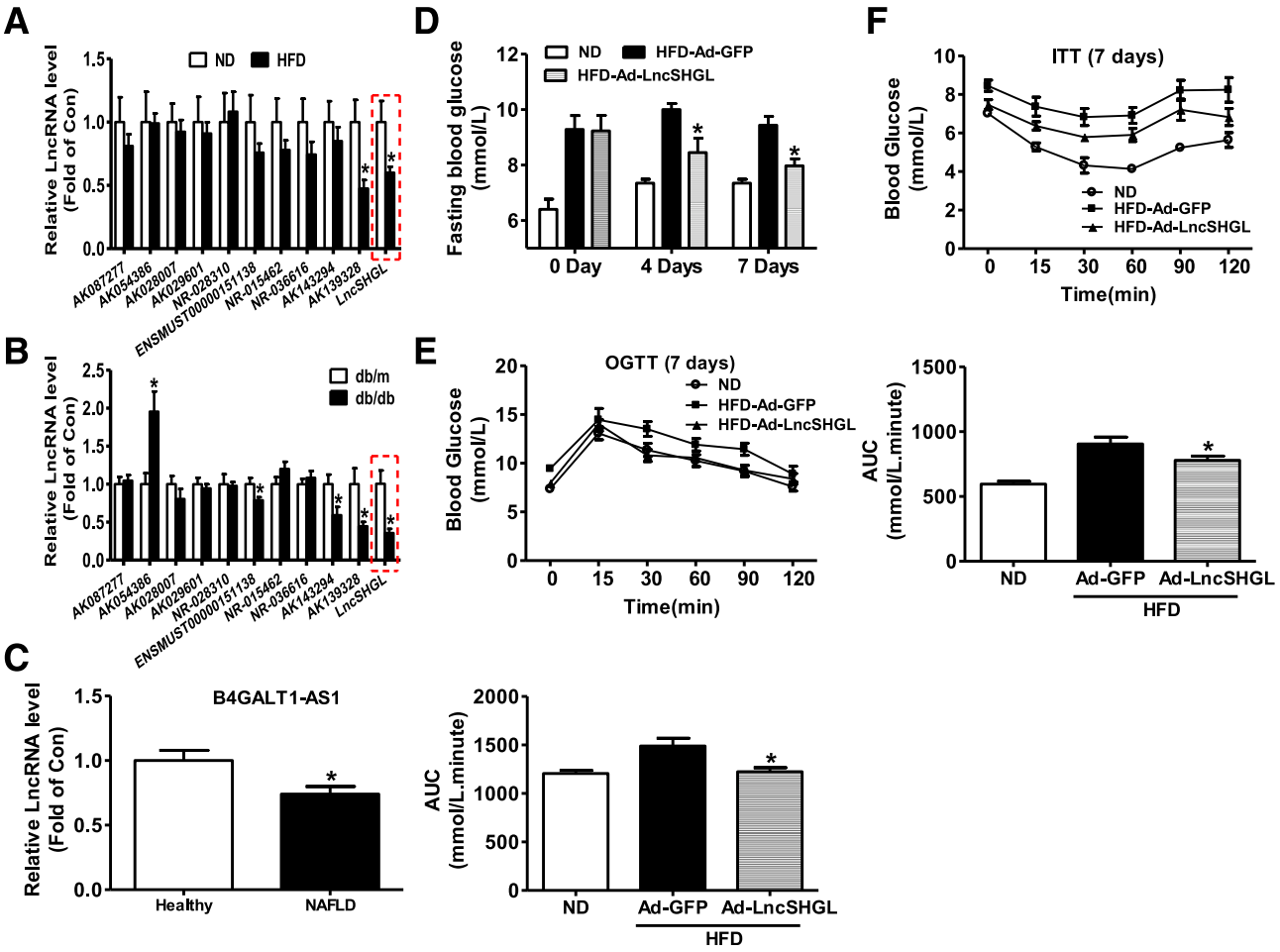

Figure 1—Hepatic lncSHGL overexpression improved glucose intolerance and insulin resistance in mice fed the HFD compared with mice fed the normal diet (ND). The expression of lncRNAs in livers of HFD mice (*A*) and in *db*/*db* mice (*B*) (n = 6–8). *P < 0.05 vs. control (Con) mice. *C*: lncRNA B4GALT1-AS1 levels were reduced in livers of subjects with nonalcoholic fatty liver disease (NAFLD) compared with healthy livers. The three B4GALT1-AS1 isoforms were detected together (n = 6). *P < 0.05 vs. healthy subjects. *D*: Fasting blood glucose levels after viral injection. *E*: OGTTs at 7th day after the viral injection. OGTT data are presented in the upper panel, and area under the curve (AUC) data are in the lower panel. *F*: ITTs at the 7th day after viral injection. ITT data are presented in the upper panel, and AUC data are in the lower panel (n = 6–8). *P < 0.05 vs. HFD mice treated with Ad-GFP.

biological function(s) also remain unknown, exhibits the best sequence match with lncSHGL (total score = 57.2, E value = 8e−5, identity = 73%). The B4GALT1-AS1 encodes three noncoding RNA isoforms. Multiple sequence alignment of lncSHGL and B4GALT1-AS1 isoforms was performed using the ClustalX tool (Supplementary Fig. 3*A*). In human livers with steatosis, total B4GALT1-AS1 levels were reduced (Fig. 1*C*). Hematoxylin and eosin staining revealed significant lipid droplet in human livers with steatosis (Supplementary Fig. 3*B*). Patients with fatty liver have higher serum triglyceride (TG) and cholesterol (CHO) levels but have similar BMI, waist circumference, liver function, and other characteristics as healthy subjects (28). Overall, a decrease in hepatic lncSHGL and B4GALT1-AS1 expression is associated with dysregulated glucose/lipid metabolism in mice and humans.

Hepatic lncSHGL Overexpression or Inhibition on Glucose and Lipid Metabolism

lncSHGL had been overexpressed in livers of HFD mice via tail vein injection of Ad-lncSHGL. Fasting hyperglycemia was improved at the 4th and 7th day after the viral injection (Fig. 1*D*). Glucose intolerance was improved at the 7th day after the viral injection (Fig. 1*E*). ITTs and hyperinsulinemic-euglycemic clamp revealed the improvement of global insulin resistance at the 7th day after the Ad-lncSHGL injection (Fig. 1*F* and Supplementary Fig. 4*A–D*). Hepatic gluconeogenesis was decreased at the 7th day after the Ad-lncSHGL injection (Supplementary Fig. 5*A* and *B*). Serum aspartate aminotransferase and alanine aminotransferase activities were not different between HFD mice treated with Ad-GFP or Ad-lncSHGL (Supplementary Fig. 5*C*). The Ad-lncSHGL injection resulted in specific lncSHGL overexpression in mouse livers (Fig. 2*A*). Morphological, Oil Red O staining, and quantitative assays indicated that lncSHGL overexpression reduced hepatic but not serum TG and CHO content (Fig. 2*B–D*). Hepatic lncSHGL overexpression reduced serum insulin levels (Fig. 2*E*). Consistent with enhanced insulin sensitivity, hepatic lncSHGL overexpression repressed the lipolysis of white adipose tissue and reduced serum FFA levels in HFD mice (Fig. 2*F*).

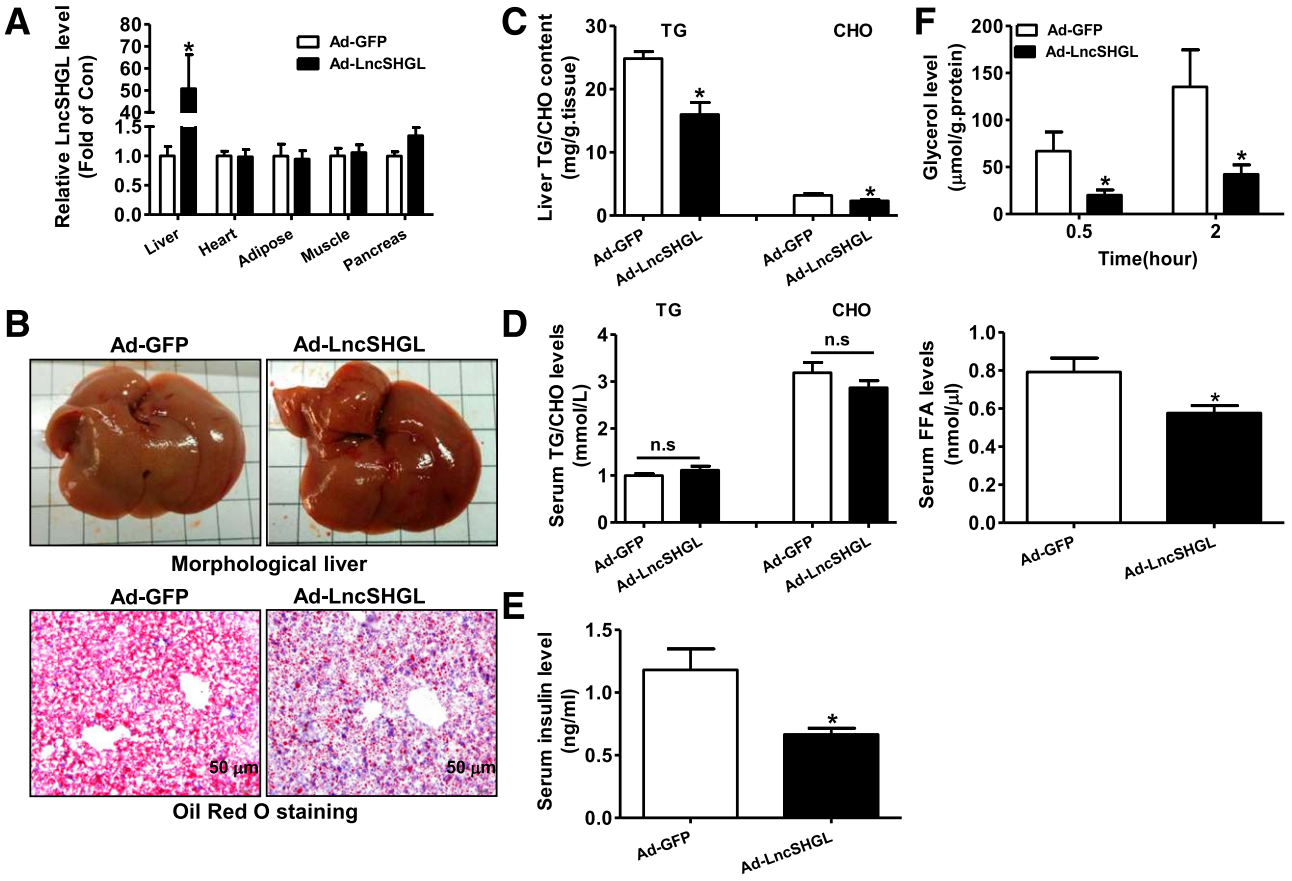

Figure 2—lncSHGL overexpression attenuated fatty liver in HFD mice. *A*: Ad-lncSHGL injection resulted in liver-specific overexpression of lncSHGL in HFD mice. *B*: Representative images of morphological and Oil Red O staining assays of HFD mouse liver after lncSHGL overexpression. *C*: lncSHGL overexpression of TG and CHO content in mouse livers. *D*: Hepatic lncSHGL overexpression of serum TG and CHO levels (n = 6–8). *$P < 0.05$ vs. control (Con) HFD mice treated with Ad-GFP. n.s., not significant. *E*: Serum insulin levels in HFD mice after hepatic lncSHGL overexpression (n = 6–8). *$P < 0.05$ vs. control mice. *F*: Hepatic lncSHGL overexpression repressed the lipolysis of epididymal adipose tissue of HFD mice (upper panel) and reduced serum FFAs levels in HFD mice (lower panel) (n = 7). Serum FFAs (C8 and longer) levels were determined using the Free Fatty Acid Quantitation Kit (Sigma-Aldrich) according to the instruction protocol. *$P < 0.05$ vs. control mice.

To confirm the metabolic roles of lncSHGL, its expression in normal C57BL/6 mouse livers was knocked down by tail vein injection of siRNAs. The injection of siRNAs specifically repressed lncSHGL expression in the livers (Fig. 3*A*). Mice treated with si-lncSHGL exhibited fasting hyperglycemia compared with control mice (Fig. 3*B*). Oil Red O staining and quantitative assays revealed that lncSHGL inhibition increased hepatic but not serum TG and CHO content (Fig. 3*C*–*E*).

lncSHGL Overexpression or Inhibition of Metabolic Gene Expression

lncSHGL overexpression increased pAkt with reduced protein levels of PEPCK, G6Pase, and fatty acid synthase (FAS) in HFD mouse livers (Fig. 4*A*). lncSHGL overexpression reduced the mRNA levels of PEPCK and G6Pase in HFD mouse livers (Fig. 4*B*). lncSHGL inhibition increased the mRNA level of PEPCK in normal mouse livers (Supplementary Fig. 6*A*). lncSHGL silencing reduced pAkt level with increased protein levels of gluconeogenic and lipogenic enzymes (Supplementary Fig. 6*B*). In HFD mouse livers, lncSHGL overexpression increased pFOXO1 but reduced pmTOR, with little effect on pGSK3 (Fig. 4*C*). Hepatic lncSHGL overexpression reduced SREBP-1C precursor protein expression in mouse livers (Fig. 4*C*). lncSHGL overexpression increased the pFOXO1 level and reduced pmTORC1 and SREBP-1C protein levels without affecting pGSK3 levels in primary mouse hepatocytes (Fig. 4*D*) and HepG2 cells (Supplementary Fig. 7*A*). Furthermore, lncSHGL overexpression reduced the levels of pS6K1 and pS6, two downstream molecules of mTORC1, and the protein level of Rictor, one of the key components of mTORC2, but had little effect on pAMPK in diabetic mouse livers (Fig. 4*C*) and primary mouse hepatocytes (Fig. 4*D*). In support of the changes in SREBP-1C and FAS protein levels, lncSHGL overexpression reduced whereas lncSHGL inhibition increased their mRNA levels in mouse livers (Supplementary Fig. 7*B* and *C*). lncSHGL overexpression increased whereas lncSHGL inhibition reduced the mRNA level of ACACB, one of the important genes controlling fatty acid oxidation, in mouse livers. In contrast, lncSHGL overexpression or silencing

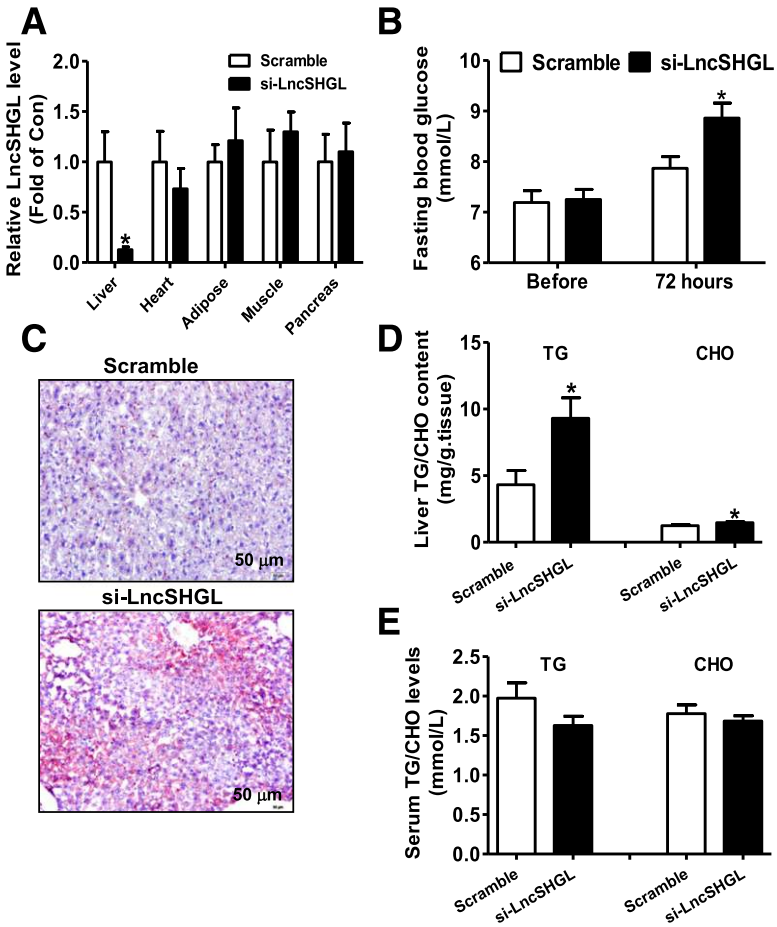

Figure 3—Hepatic lncSHGL inhibition promoted fasting hyperglycemia and lipid deposition in C57BL/6 mice. *A*: si-lncSHGL injection reduced lncSHGL levels in C57BL/6 mouse livers. *B*: Hepatic lncSHGL inhibition elevated fasting blood glucose levels in normal C57BL/6 mice. Blood glucose levels were monitored at 72 h after siRNA injection. *C*: Oil Red O staining of liver samples treated with si-lncSHGL or scrambled siRNA (scramble). *D*: Hepatic lncSHGL inhibition increased liver TG and CHO content. *E*: Hepatic lncSHGL had little effect on serum TG and CHO levels (n = 8–10). *$P < 0.05$ vs. control (Con) mice treated with scrambled siRNA.

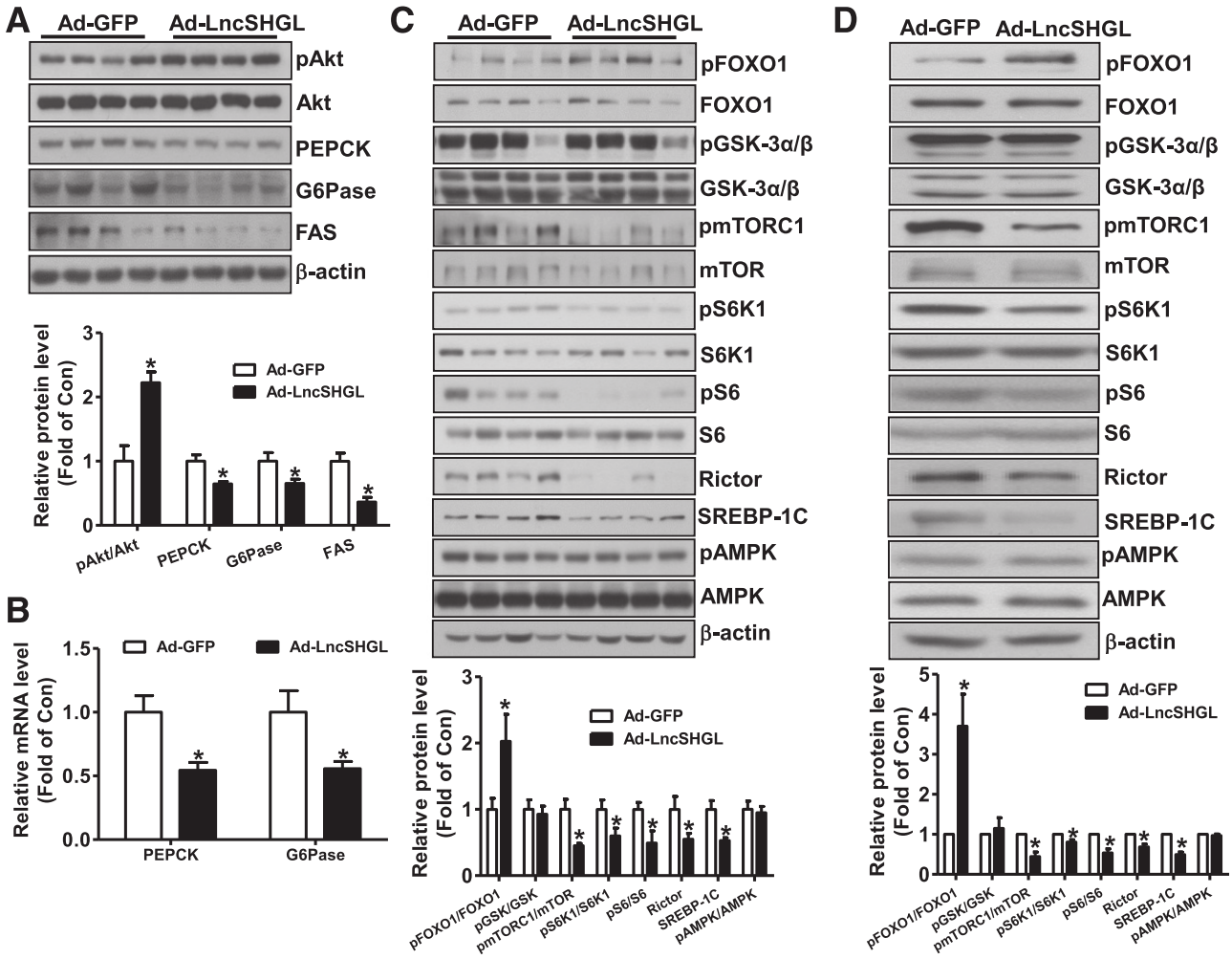

Figure 4—The effects of lncSHGL overexpression on gluconeogenic/lipogenic gene expression in HFD mouse livers and primary hepatocytes. *A*: lncSHGL overexpression reduced the protein levels of gluconeogenic and lipogenic genes in HFD mouse livers. Representative gel images are presented in the upper panel, and quantitative data are in the lower panel. *B*: lncSHGL overexpression on the mRNA levels of gluconeogenic genes in HFD mouse livers. *C*: Effect of lncSHGL overexpression on protein levels of metabolic genes in HFD mouse livers. Representative gel images are shown in the upper panel, and quantitative data are in the lower panel (n = 6–8). SREBP-1C is full-length SREBP-1C protein. *$P <$ 0.05 vs. control (Con) mice. *D*: Effect of lncSHGL overexpression on the protein levels of metabolic genes in primary mouse hepatocytes. Representative gel images are shown in the upper panel, and quantitative data are in the lower panel (n = 3–5). Phosphorylation of FOXO1 at Ser256, GSK3α/β at Ser21/Ser9, mTOR at Ser2448, p70 S6 kinase (S6K1) at Thr389, S6 ribosomal protein at Ser235/Ser236, and AMPKα at Thr172 was analyzed, respectively. *$P < 0.05$ vs. control cells.

had little effect on the mRNA levels of SCD1, DGAT1, AOX, ApoB, FABP1, CPT1α, and PDK4 in mouse livers (Supplementary Fig. 7*B* and *C*). Overall, these findings revealed that lncSHGL suppressed hepatic lipogenesis and likely increased lipid oxidation.

lncSHGL Promoted Akt Activation and FOXO1 Nuclear Exclusion in CaM-Dependent Manner

Because Akt activity and its downstream molecules were changed after lncSHGL overexpression or inhibition in mouse livers, whether lncSHGL directly modulated Akt activity was further evaluated in cultured hepatocytes. lncSHGL overexpression in HepG2 cells promoted Akt activation independent of insulin (Fig. 5*A*). lncSHGL-induced Akt activation was blocked by inhibitors of PI3K (wortmannin) and CaM (CPZ) but was not affected by inhibitors of P2 receptors (Fig. 5*B*), L-type calcium channel, and inositol trisphosphate receptor (IP3R) (Supplementary Fig. 8*A*). lncSHGL had little effect on the cellular Ca^{2+} level (Supplementary Fig. 8*B*), and depleting extracellular calcium failed to affect its stimulatory effect on Akt phosphorylation in HepG2 cells (Fig. 5*C*). However, lncSHGL-induced Akt activation was completely blocked by the CaM inhibitor in the presence or absence of extracellular calcium in HepG2 cells (Fig. 5*C*). lncSHGL similarly activated Akt in an insulin-independent but CaM-dependent manner in primary mouse hepatocytes (Supplementary Fig. 9*A* and Fig. 5*D*). lncSHGL promoted FOXO1 nuclear exclusion in a CaM-dependent manner in HepG2 cells (Fig. 5*E*) and mouse hepatocytes (Supplementary Fig. 9*B*). lncSHGL repressed gluconeogenic gene expression and gluconeogenesis in HepG2 cells (Fig. 5*F*) and mouse

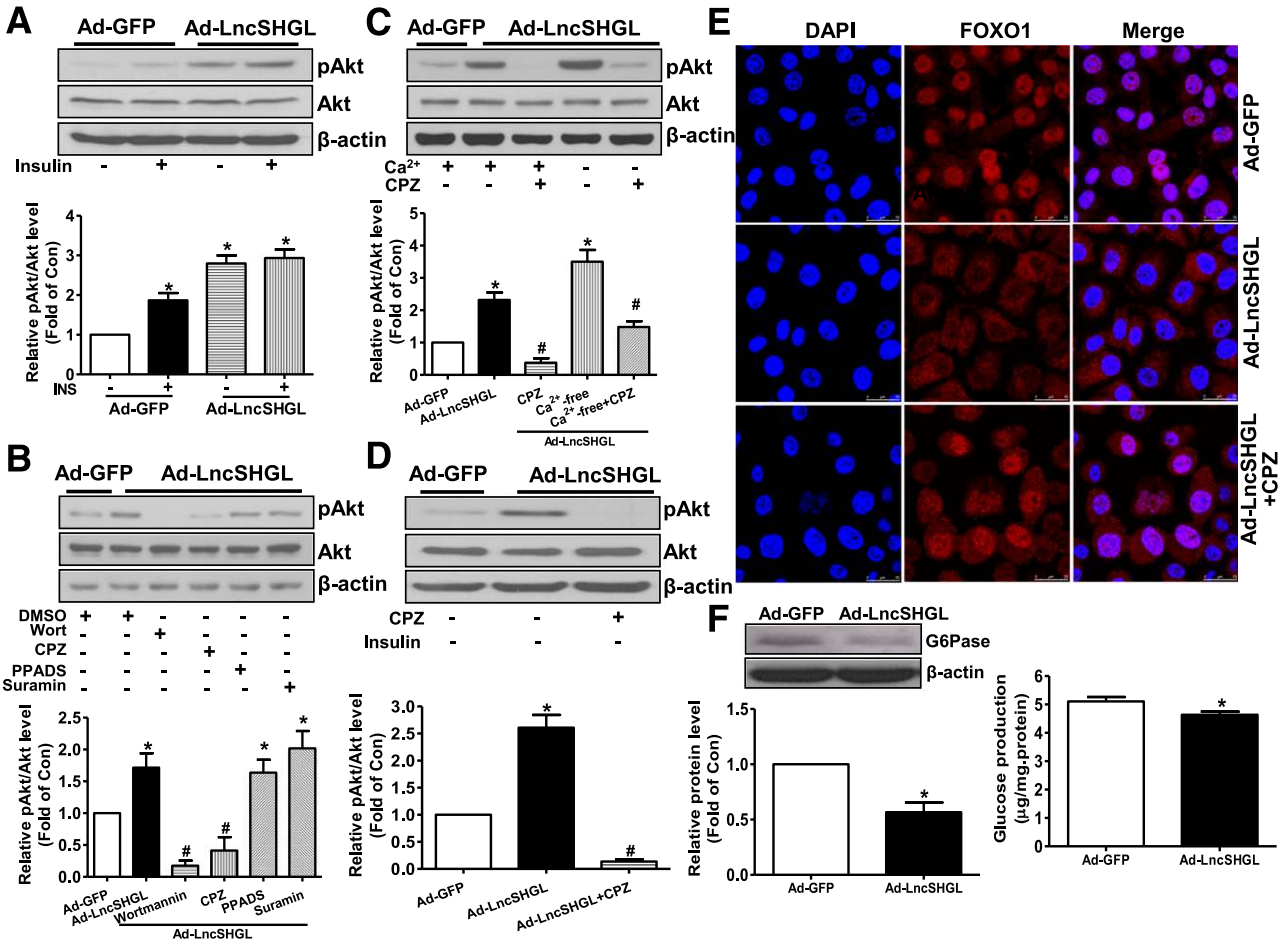

Figure 5—lncSHGL promoted Akt activation and FOXO1 nuclear exclusion in a CaM-dependent manner in hepatocytes. *A*: lncSHGL induced Akt activation in an insulin-independent manner in HepG2 cells. Cells infected with Ad-GFP or Ad-lncSHGL were serum starved for 12 h and then stimulated with 100 nmol/L insulin for 5 min before the pAkt level was analyzed ($n = 3$). *$P < 0.05$ vs. control (Con) cells treated with Ad-GFP without insulin stimulation. *B*: lncSHGL activated Akt via a PI3K- and CaM-dependent manner in HepG2 cells. Ad-lncSHGL–infected cells were treated with wortmannin (Wort; 1 μmol/L) and CPZ (100 μmol/L) for 1 h before the pAkt level was analyzed ($n = 3$–5). *$P < 0.05$ vs. Ad-GFP–treated cells; #$P < 0.05$ vs. Ad-lncSHGL–treated cells without inhibitor treatment. *C*: lncSHGL-induced Akt activation was not dependent on influx of extracellular calcium. At 24 h after infection, cell culture medium was replaced with calcium-free medium plus 0.5 mmol/L EGTA for 2 h, and CPZ was added 1 h before the experimental assay ($n = 3$–5). *$P < 0.05$ vs. Ad-GFP–treated cells; #$P < 0.05$ vs. Ad-lncSHGL–treated cells or Ca^{2+}-free cells without CPZ treatment. *D*: lncSHGL induced Akt activation in a CaM-dependent manner in primary mouse hepatocytes ($n = 3$–5). *$P < 0.05$ vs. Ad-GFP–treated cells; #$P < 0.05$ vs. Ad-lncSHGL–treated cells without inhibitor treatment. *E*: lncSHGL promoted nuclear exclusion of FOXO1 in a CaM-dependent manner in HepG2 cells. Scale bar = 25 μm. *F*: lncSHGL overexpression reduced G6Pase protein level (left panel) and repressed glucose production (right panel) in HepG2 cells ($n = 3$–5). *$P < 0.05$ vs. Ad-GFP–treated cells.

hepatocytes (Supplementary Fig. 9*C* and *D*). Overall, lncSHGL activated the PI3K/Akt pathway in an insulin-independent but CaM-dependent manner.

lncSHGL Recruited hnRNPA1 to Enhance Calmodulin mRNA Translation

To further determine the CaM-dependent mechanism of Akt activation induced by lncSHG, its effect on CaM expression was analyzed. Three calmodulin genes, designated as CALM1, CALM2, and CALM3, respectively, encode one identical CaM protein (35). lncSHGL overexpression increased whereas lncSHGL silencing decreased CaM protein level with little effect on CALM1-3 mRNA levels in mouse livers (Fig. 6*A* and *B*). lncSHGL overexpression also increased the CaM protein level without affecting CALM1-3 mRNA levels in mouse hepatocytes (Fig. 6*C*) and HepG2 cells (Fig. 6*D* and *E*). In HFD mouse livers, lncSHGL overexpression had little effect on the ubiquitination of CaM protein (Supplementary Fig. 10). CALM2 plasmid transfection activated Akt independent of insulin in HepG2 cells (Fig. 6*F*). lncSHGL clearly increased CaM protein to induce Akt activation in hepatocytes. Moreover, CaM overexpression reduced pmTORC1 and SREBP-1C protein levels in mouse hepatocytes (Supplementary Fig. 11*A*). CaM interacted with mTOR, and the interaction was increased after lncSHGL and CaM overexpression in mouse hepatocytes (Supplementary Fig. 11*B* and *C*).

An RNA pull-down assay was performed to further pinpoint the mechanism(s) of the lncSHGL-induced

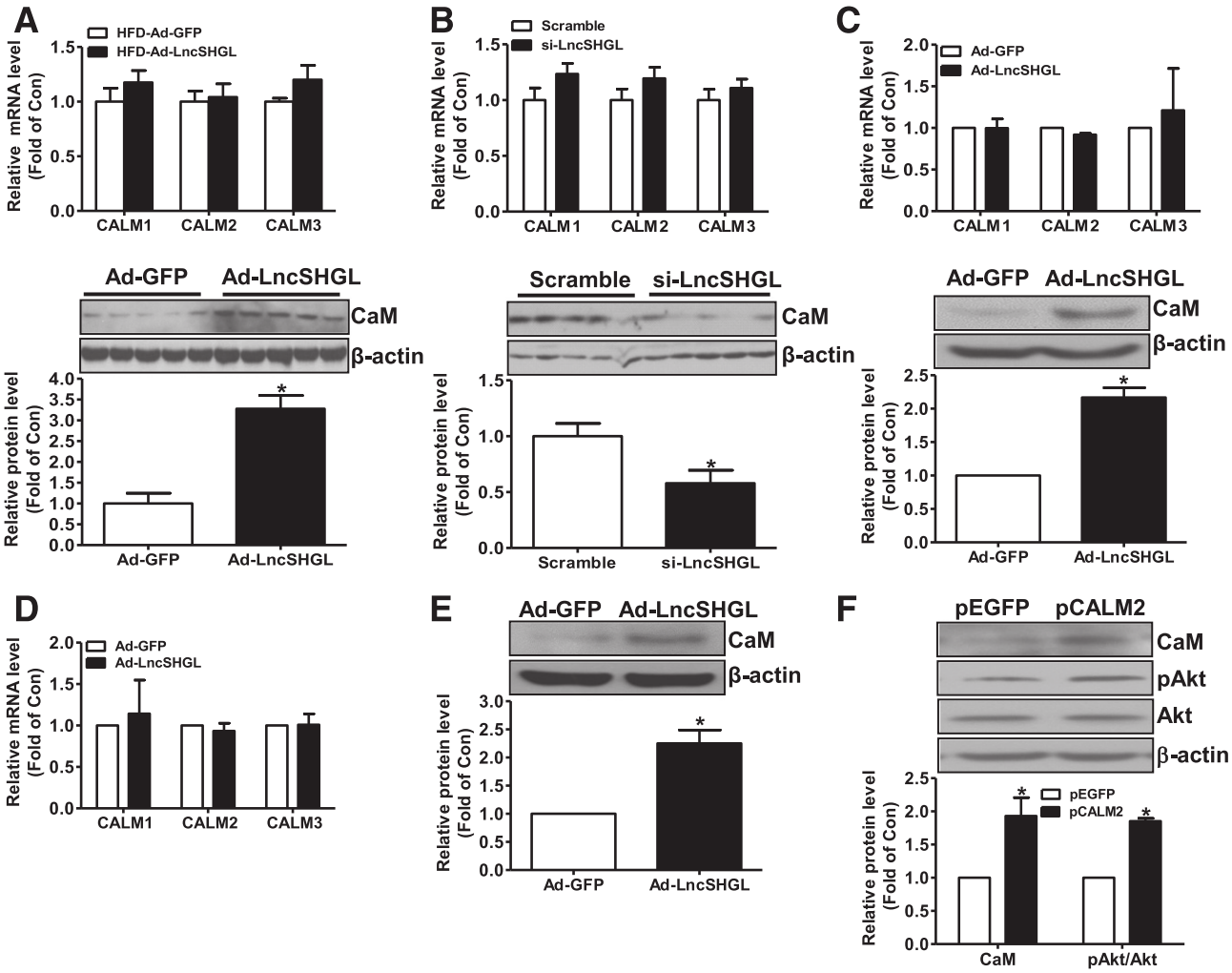

Figure 6—lncSHGL increased CaM protein levels without affecting CaM mRNA levels. *A*: Effect of lncSHGL overexpression on the mRNA levels of CALM1-3 and the protein level of CaM in HFD mouse livers ($n = 6$). *$P < 0.05$ vs. control (Con) mouse livers. *B*: Effect of lncSHGL silencing on the mRNA levels of CALM1-3 and the protein level of CaM in C57BL/6 mouse livers ($n = 6$). *$P < 0.05$ vs. control mouse livers. *C*: Effect of lncSHGL overexpression on CALM1-3 mRNA levels and CaM protein level in primary mouse hepatocytes ($N = 3–5$). *$P < 0.05$ vs. control mouse hepatocytes. *A–C*: The mRNA data are presented in the upper panels and the protein data are in the lower panels. *D*: lncSHGL overexpression had little effect on the mRNA levels of CALM1-3 in HepG2 cells. *E*: lncSHGL overexpression increased the CaM protein level in HepG2 cells ($n = 3–5$). *$P < 0.05$ vs. control cells. *F*: Plasmid overexpression of CALM2 activated Akt independent of insulin in HepG2 cells ($n = 3–5$). *$P < 0.05$ vs. control cells.

increase in the CaM protein level in liver cells. MS analysis had identified hnRNPA1 as the target protein of the indicated band in Fig. 7*A* (MS data are reported in Supplementary Table 3). Immunoblotting assay confirmed that lncSHGL interacted with hnRNPA1 in NCTC cells (Fig. 7*B*). lncSHGL overexpression increased the lncSHGL-hnRNPA1 interaction without significantly affecting the hnRNPA1 protein level (Fig. 7*B*). RIP revealed that hnRNPA1 bound with CALM1-3 mRNAs and that the bindings were enhanced by lncSHGL overexpression in NCTC cells (Fig. 7*C*). lncSHGL overexpression also increased the bindings of ribosomes with CALM1-3 mRNAs (Fig. 7*D*). hnRNPA1 overexpression increased CaM and pAkt protein levels with little effect on CALM1-3 mRNA levels in primary mouse hepatocytes (Fig. 7*E* and *F*) and HepG2 cells (Supplementary Fig. 12*A* and *B*), whereas hnRNPA1 silencing reduced CaM and pAkt protein levels without a significant effect on CALM1-3 mRNA levels in HepG2 cells (Supplementary Fig. 13*A* and *B*). hnRNPA1 knockdown inhibited the lncSHGL-induced increase in CaM and pAkt levels without a significant effect on CALM1-3 mRNA levels (Supplementary Fig. 13*C* and *D*). Consistent with the changes in CaM and pAkt levels, hnRNPA1 silencing increased glucose production and impaired repression of lncSHGL on glucose production in HepG2 cells (Supplementary Fig. 13*E*).

Hepatic overexpression of hnRNPA1 and CaM ameliorated hyperglycemia and steatosis of HFD mice (Fig. 8*A* and *B*). hnRNPA1 overexpression increased the CaM protein level without a significant effect on CALM1-3 mRNA levels

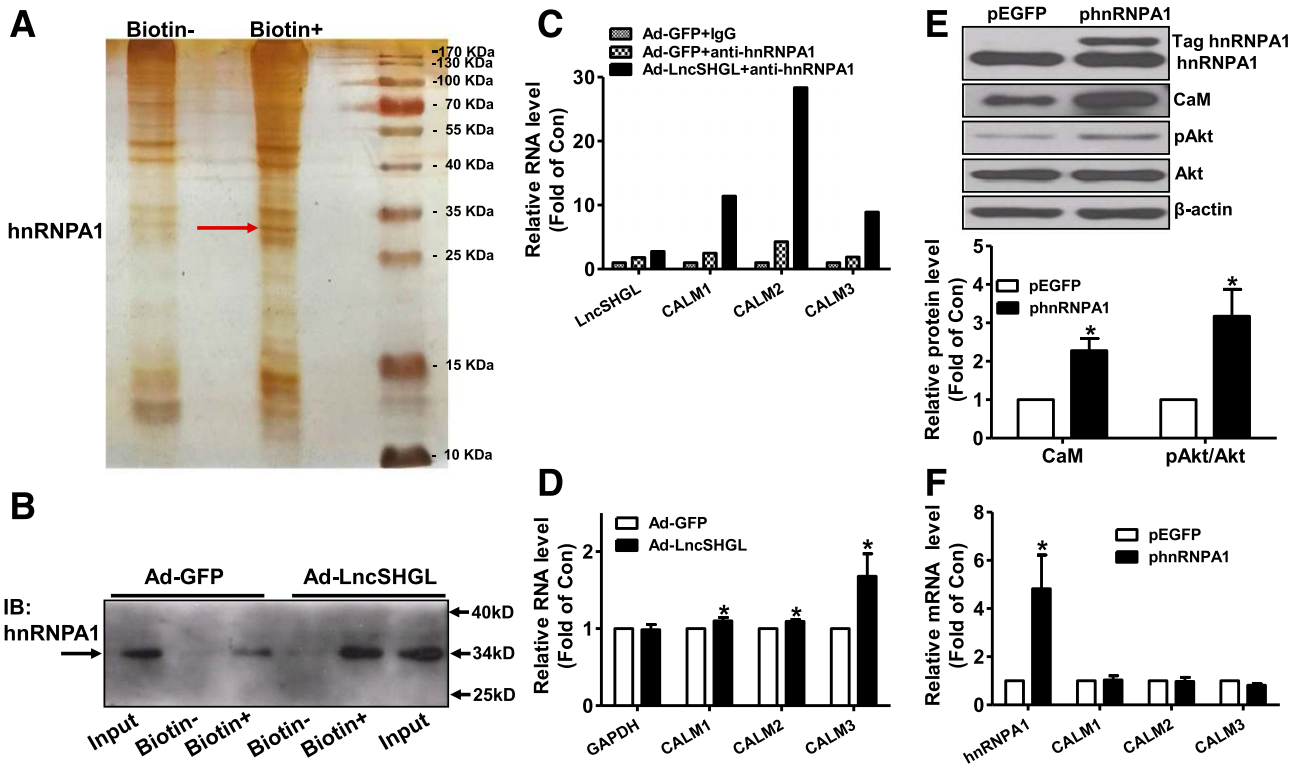

Figure 7—lncSHGL recruited hnRNPA1 to enhance the translation efficiency of CALM mRNAs in liver cells. *A*: RNA pull-down experiment revealed that lncSHGL interacted with hnRNPA1 in normal liver NCTC-1469 cells. MS analyses had identified the indicated band as hnRNPA1. *B*: Western blotting analyses confirmed the interaction between lncSHGL and hnRNPA1 in NCTC-1469 cells. Biotin–, RNA pull-down using nonbiotin-labeled PCR products; Biotin+, RNA pull-down using biotin-labeled PCR products; IB, immunoblotting; Input, cell lysate as a positive control. *C*: RNA immunoprecipitation revealed that hnRNPA1 was bound with CALM1-3 mRNAs in NCTC-1469 cells. The data are presented as the mean value of three independent experiments. *D*: lncSHGL overexpression increased the binding of ribosomes with CALM1-3 mRNAs in NCTC-1469 cells (n = 4–5). The housekeeping gene GAPDH was used as a control. *$P < 0.05$ vs. Ad-GFP-treated cells. hnRNPA1 overexpression on CALM1-3 mRNA levels (*E*) and CaM protein level (*F*) in primary mouse hepatocytes (n = 3–5). *$P < 0.05$ vs. pEGFP-transfected control cells. Con, control.

in HFD mouse livers (Fig. 8*C* and *D*). hnRNPA1 overexpression activated Akt and reduced pmTORC1 and SREBP-1C levels with the repression of gluconeogenic and lipogenic gene expression (Fig. 8*C*). hnRNPA1 overexpression also reduced pS6K1 and pS6, and Rictor protein levels in HFD mouse livers (Supplementary Fig. 14*A*).

CaM overexpression also increased pAkt level with repressed gluconeogenic and lipogenic expression in HFD mouse livers (Supplementary Fig. 14*B* and *C*). The expression levels of lncSHGL and CaM and pAkt proteins were reduced in fasting mouse livers but were restored after refeeding (Supplementary Fig. 15*A* and *C*).

DISCUSSION

Insulin physiologically activates Akt through the insulin receptor/PI3K pathway to inactivate FOXO1 by phosphorylating and promoting its nuclear exclusion. Excessive FOXO1 activation due to insulin resistance or deficiency promotes hepatic gluconeogenesis and fasting hyperglycemia (36–38). Deletion of hepatic FOXO1 rescues hyperglycemia by repressing gluconeogenic gene expression in mice with liver-specific knockout of the insulin receptor (39). Moreover, FOXO1 also induces the expression in the liver of lipogenic genes such as FAS and PANDER (24,40). Transgenic or Ad overexpression of FOXO1 in the liver promoted lipid deposition (24,40). Under severe insulin resistance, inactivating hepatic FOXO1 via insulin-independent mechanism(s) holds great promise for the treatment of type 2 diabetes and fatty liver.

Gain- and loss-of-function studies revealed that lncSHGL suppresses hepatic gluconeogenesis and lipogenesis. In the previous studies, we reported that the ATP-P2 receptor signaling–mediated increase in cellular calcium level functionally activates CaM to induce Akt activation and suppress hepatic gluconeogenesis and lipogenesis in obese diabetic mice (22,23). These previous findings had established an insulin-independent but calcium-dependent activation of the CaM/Akt metabolic pathway. We also found that FAM3C activates HSF1 to directly induce CALM1 transcription and elevate the CaM protein level to activate the Akt pathway in a Ca^{2+}-independent manner (26). The current study further revealed that lncSHGL modulates the CaM protein level at the posttranscriptional level to induce Akt activation. lncSHGL also inhibits mTORC1 and

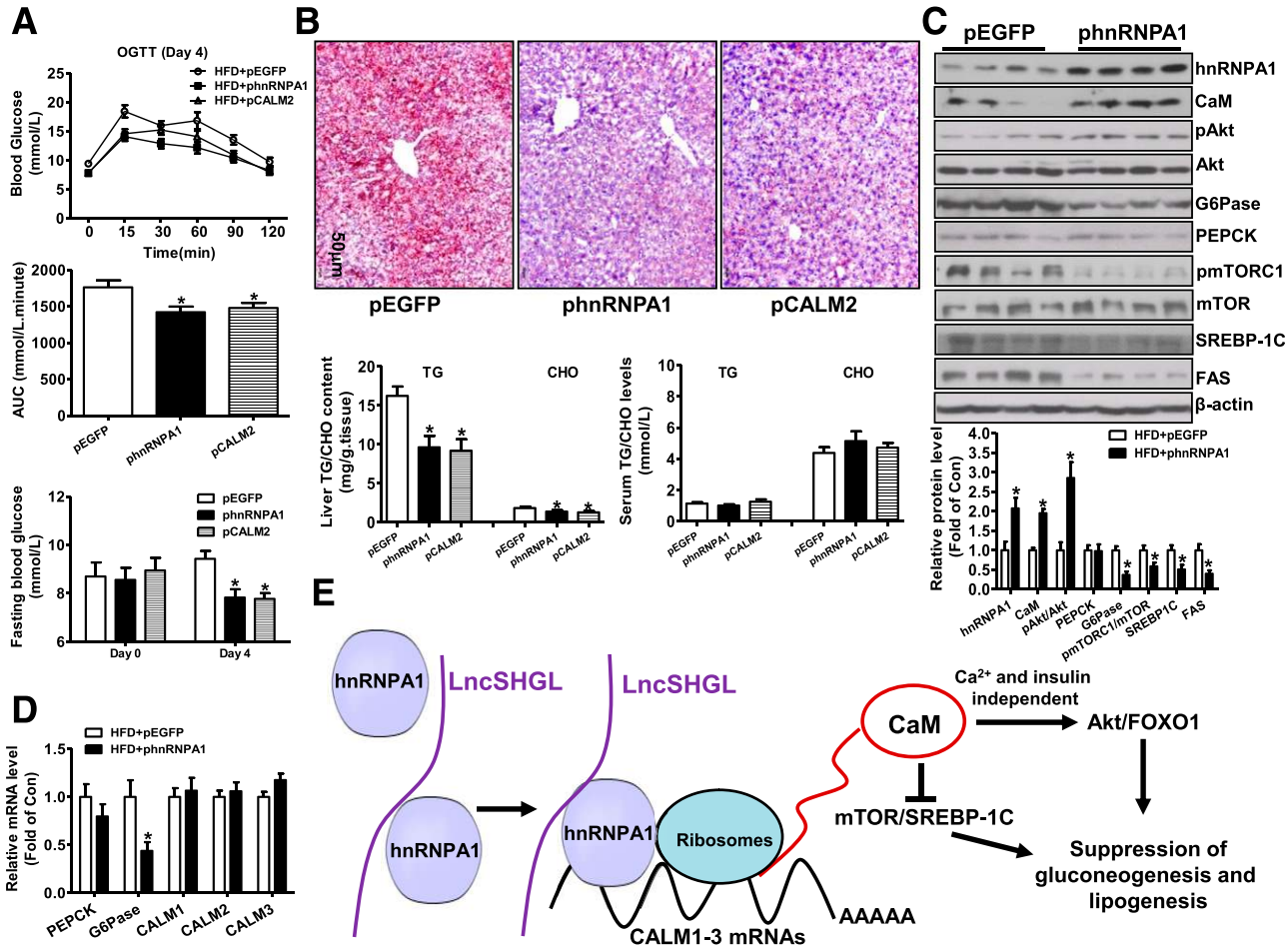

Figure 8—Hepatic hnRNPA1 and CaM overexpression improved hyperglycemia and fatty liver in HFD mice. *A*: OGTT at 72 h after plasmid injection. OGTT data are presented in the upper panel, area under the curve (AUC) data are in the middle panel, and fasting blood glucose levels before and after the plasmid injection are in the lower panel (N = 8–10). *$P < 0.05$ vs. control mice. *B*: hnRNPA1 and CALM2 overexpression ameliorated fatty liver in HFD mice. Representative images of Oil Red O staining are shown in the upper panel, and quantitative TG and CHO levels in mouse livers and serum are shown in the lower panels (n = 8–10). *$P < 0.05$ vs. control mice. *C*: Effect of hnRNPA1 overexpression on the protein levels of metabolic genes in HFD mouse livers. Representative gel images are presented in the upper panel and quantitative data in the lower panel (n = 6–8). *$P < 0.05$ vs. control (Con) mice. *D*: Effect of hnRNPA1 overexpression on the mRNA levels of metabolic genes in HFD mice (n = 8–10). *$P < 0.05$ vs. control mice livers. *E*: Proposed mechanism of lncSHGL in suppressing hepatic gluconeogenesis and lipogenesis. lncSHGL recruited hnRNPA1 to enhance the translation efficiency of CALM1-3 mRNAs, thus elevating the cellular CaM protein level. An increase in CaM protein level activates the Akt pathway and represses the mTOR/SREBP-1C pathway to suppress gluconeogenesis and lipogenesis in hepatocytes.

mTORC2 pathways, which promote hepatic lipid deposition (41). That lncSHGL activates Akt but represses mTOR pathways in hepatocytes is clear; thus far, however, the mechanism of lncSHGL's inhibition effect on mTOR pathways in hepatocytes remains unclear. lncSHGL likely elevates CaM protein to repress pmTOR via a direct interaction. Similarly, FAM3C activates HSF1 to induce CALM1 transcription, elevating CaM protein to activate Akt independent of calcium. However, FAM3C also represses the mTORC1 pathway with unknown mechanism(s) in hepatocytes (26).

Although Akt activates mTOR in hepatocytes (42), our findings revealed a new regulatory network in which an increase in CaM protein activates the Akt pathway and represses mTOR pathways in hepatocytes (Fig. 8*E*). CaM regulates many physiological and pathophysiological processes by interacting with hundreds of target proteins (43). CaM is generally activated by an increase in cellular Ca^{2+} level (22,23); however, CaM also interacts with its targets via a Ca^{2+}-independent manner in some conditions (43). The upstream signals determine the interaction between CaM and its target proteins in various conditions (43). CaM has been reported to interact and activate mTORC1 in a Ca^{2+}-dependent manner in HEK293 cells (44). Our previous and current findings suggested that transcriptional and translational upregulation of the CaM protein level represses the mTOR pathway via a Ca^{2+}-independent mechanism in hepatocytes (26). That CaM interacts with mTOR to repress or activate it likely depends on upstream and cellular Ca^{2+} signals in various cell types.

Insulin resistance also plays important roles in the development of fatty liver by promoting lipid transfer from adipose tissue to the liver (ectopic fat deposition) (45).

Overall, the repression of FOXO1 and mTOR/SREBP-1C pathways and the improvement of global insulin resistance together contribute to the beneficial effects of lncSHGL on fatty liver. Moreover, a reduction in lncSHGL expression may exert a deleterious effect on liver IRI observed in our previous studies (7,8) by impairing Akt activity.

hnRNPA1 is an RNA-binding protein regulating the translation efficiency of mRNAs (46). Although we found that hnRNPA1 promotes Akt activation, Akt also phosphorylates hnRNPA1 (47), revealing a cross-regulation between hnRNPA1 and Akt activities. Several recent lines of evidence suggest that hnRNPA1 plays important roles in regulating glucose and lipid metabolism. FFAs stimulate the expression of hnRNPA1, which binds to SREBP-1a mRNA and increases its translation in HepG2 cells (48). hnRNPA1 also splices glycolytic enzyme pyruvate kinase precursor mRNA to form mature pyruvate kinase isoform 2 (PKM2) mRNA (49,50). In omental adipose tissue of morbidly obese patients, hnRNPA1 expression is decreased (51). Moreover, hnRNPA1 is also associated with insulin receptor gene splicing in adipose tissue of humans with body weight loss (52).

We previously showed that the CaM protein level is reduced in obese mouse livers due to transcription repression of CALM1 (26). The current study revealed that lncSHGL recruited hnRNPA1 to enhance the translation efficiency of CALM mRNAs without affecting their transcription in hepatocytes. Clearly, the inhibition at the transcriptional and translational levels of CALM1-3 mRNAs together contributes to the decreased hepatic CaM protein under the obese state (26). Beyond the transcriptional regulation of CALM genes by transcription factors such as HSF1 (26), modulating the translation efficiency of CALM mRNAs by the lncSHGL/hnRNPA1 axis is also important for maintaining CaM protein level, Akt activity, and glucose/lipid homeostasis in the basal condition when the insulin level is low in hepatocytes. Administration of CPZ, an inhibitor of CaM, had been reported to induce hyperglycemia with unclear mechanism(s) (53). Our previous (22,23,28) plus current findings suggested that the enhancement of hepatic gluconeogenesis induced by inhibiting the CaM/Akt pathway is a novel mechanism for explaining the hyperglycemic effect of CPZ. Our previous (26) and current findings revealed that an increase in CaM protein triggered by transcriptional or posttranscriptional mechanisms activates the PI3K/Akt pathway and represses the mTOR pathway in hepatocytes independent of calcium. These findings shed light on the Ca^{2+}-independent action modes of CaM. Overall, the lncSHGL/hnRNPA1 axis plays important roles in suppressing hepatic gluconeogenesis and lipogenesis via the modulation of CaM protein levels at the posttranscriptional level.

Moreover, we identified human lncRNA B4GALT1-AS1 as the homologous sequence of mouse lncSHGL. Although B4GALT1-AS1 levels were reduced in steatotic human livers, we regret that we were not able to analyze the CaM protein level due to the unavailability of sufficient human liver samples. However, SREBP-1 and FAS expression were increased in steatotic human livers in the previous study (33). The lncSHGL/hnRNPA1/CaM pathway is also involved in regulating Akt activity and hepatic glucose production in physiological conditions such as fasting/refeeding. Repression of the lncSHGL/hnRNPA1/CaM axis for a short time is likely beneficial for increasing gluconeogenesis in fasting status; however, long-term inhibition triggers fasting hyperglycemia and steatosis under the obese state. Regarding the roles of lncSHGL in regulating hepatic glucose/lipid metabolism, several issues should be noted. That lncSHGL also recruits hnRNPA1 to regulate the translation efficiency of other mRNA(s) beyond CALM1-3 mRNAs is also possible. To further identify the target mRNAs of the lncSHGL/hnRNPA1 axis is of great significance. lncSHGL may also regulate hepatic glucose and lipid metabolism via other mechanism(s) beyond hnRNPA1/CaM pathway.

In summary, the new lncRNA lncSHGL recruits hnRNPA1 to enhance the translation efficiency of CALM mRNAs without affecting their transcription, elevating CaM protein level to suppress hepatic gluconeogenesis/lipogenesis independent of insulin and calcium (Fig. 8*E*). Activating lncSHGL/hnRNPA1 axis represents a potential strategy for the treatment of type 2 diabetes and steatosis.

Funding. This study was supported by grants from National Key Research Program of China (2016YFC1304803 and 2017YFC0909600), the Natural Science Foundation of China (81670748, 81471035, 81322011, 81670462, and 81422006), and Beijing Natural Science Foundation (7171006).

Duality of Interest. No potential conflicts of interest relevant to this article were reported.

Author Contributions. J.W. and W.Y. wrote the manuscript. J.W., W.Y., and Z.C. researched data and contributed to discussion. J.W., W.Y., Q.C., and J.Y. designed the study and revised and edited the manuscript. J.C., Y.M., and B.F. provided the technical assistance and animal model preparation. L.S., L.D., and J.L. provided human liver samples and contributed to discussion. Q.C. and J.Y. are the guarantors of this work and had full access to all the data in the study and take responsibility for the integrity of the data and the accuracy of the data analysis.

References

1. ENCODE Project Consortium. An integrated encyclopedia of DNA elements in the human genome. Nature 2012;489:57–74

2. Yue F, Cheng Y, Breschi A, et al.; Mouse ENCODE Consortium. A comparative encyclopedia of DNA elements in the mouse genome. Nature 2014;515:355–364

3. Bertone P, Stolc V, Royce TE, et al. Global identification of human transcribed sequences with genome tiling arrays. Science 2004;306:2242–2246

4. Kapranov P, Cheng J, Dike S, et al. RNA maps reveal new RNA classes and a possible function for pervasive transcription. Science 2007;316:1484–1488

5. Mattick JS, Makunin IV. Non-coding RNA. Hum Mol Genet 2006;15:R17–R29

6. Huarte M. The emerging role of lncRNAs in cancer. Nat Med 2015;21:1253–1261

7. Chen Z, Jia S, Li D, et al. Silencing of long noncoding RNA AK139328 attenuates ischemia/reperfusion injury in mouse livers. PLoS One 2013;8:e80817

8. Chen Z, Luo Y, Yang W, et al. Comparison analysis of dysregulated LncRNA profile in mouse plasma and liver after hepatic ischemia/reperfusion injury. PLoS One 2015;10:e0133462

9. Li D, Chen G, Yang J, et al. Transcriptome analysis reveals distinct patterns of long noncoding RNAs in heart and plasma of mice with heart failure. PLoS One 2013;8:e77938

10. Tang J, Jiang R, Deng L, Zhang X, Wang K, Sun B. Circulation long non-coding RNAs act as biomarkers for predicting tumorigenesis and metastasis in hepatocellular carcinoma. Oncotarget 2015;6:4505–4515
11. Prasanth KV, Spector DL. Eukaryotic regulatory RNAs: an answer to the 'genome complexity' conundrum. Genes Dev 2007;21:11–42
12. Geisler S, Coller J. RNA in unexpected places: long non-coding RNA functions in diverse cellular contexts. Nat Rev Mol Cell Biol 2013;14:699–712
13. Lee JT. Epigenetic regulation by long noncoding RNAs. Science 2012;338: 1435–1439
14. Quinn JJ, Chang HY. Unique features of long non-coding RNA biogenesis and function. Nat Rev Genet 2016;17:47–62
15. Li J, Ma W, Zeng P, et al. LncTar: a tool for predicting the RNA targets of long noncoding RNAs. Brief Bioinform 2015;16:806–812
16. Morán I, Akerman I, van de Bunt M, et al. Human β cell transcriptome analysis uncovers lncRNAs that are tissue-specific, dynamically regulated, and abnormally expressed in type 2 diabetes. Cell Metab 2012;16:435–448
17. Yin DD, Zhang EB, You LH, et al. Downregulation of lncRNA TUG1 affects apoptosis and insulin secretion in mouse pancreatic β cells. Cell Physiol Biochem 2015;35:1892–1904
18. Kallen AN, Zhou XB, Xu J, et al. The imprinted H19 lncRNA antagonizes let-7 microRNAs. Mol Cell 2013;52:101–112
19. Gao Y, Wu F, Zhou J, et al. The H19/let-7 double-negative feedback loop contributes to glucose metabolism in muscle cells. Nucleic Acids Res 2014;42: 13799–13811
20. Li P, Ruan X, Yang L, et al. A liver-enriched long non-coding RNA, lncLSTR, regulates systemic lipid metabolism in mice. Cell Metab 2015;21:455–467
21. Zhu X, Wu YB, Zhou J, Kang DM. Upregulation of lncRNA MEG3 promotes hepatic insulin resistance via increasing FoxO1 expression. Biochem Biophys Res Commun 2016;469:319–325
22. Wang C, Chen Z, Li S, et al. Hepatic overexpression of ATP synthase β subunit activates PI3K/Akt pathway to ameliorate hyperglycemia of diabetic mice. Diabetes 2014;63:947–959
23. Wang C, Chi Y, Li J, et al. FAM3A activates PI3K p110α/Akt signaling to ameliorate hepatic gluconeogenesis and lipogenesis. Hepatology 2014;59:1779–1790
24. Li J, Chi Y, Wang C, et al. Pancreatic-derived factor promotes lipogenesis in the mouse liver: role of the Forkhead box 1 signaling pathway. Hepatology 2011;53: 1906–1916
25. Golinski M, DeLaLuz PJ, Delcamp TJ, Watt DS, Vanaman TC. Synthesis and binding affinity of bidentate phenothiazines with two different photoactive groups. Bioconjug Chem 1995;6:567–572
26. Chen Z, Ding L, Yang W, et al. Hepatic activation of the FAM3C-HSF1-CaM pathway attenuates hyperglycemia of obese diabetic mice. Diabetes 2017;66:1185–1197
27. Rinn JL, Kertesz M, Wang JK, et al. Functional demarcation of active and silent chromatin domains in human HOX loci by noncoding RNAs. Cell 2007;129:1311–1323
28. Yang W, Wang J, Chen Z, et al. NFE2 induces miR-423-5p to promote gluconeogenesis and hyperglycemia by repressing the hepatic FAM3A-ATP-Akt pathway. Diabetes 2017;66:1819–1832
29. Tang H, Fan X, Xing J, et al. NSun2 delays replicative senescence by repressing p27 (KIP1) translation and elevating CDK1 translation. Aging (Albany NY) 2015;7: 1143–1158
30. Liu F, Song Y, Liu D. Hydrodynamics-based transfection in animals by systemic administration of plasmid DNA. Gene Ther 1999;6:1258–1266
31. Tsai WC, Hsu SD, Hsu CS, et al. MicroRNA-122 plays a critical role in liver homeostasis and hepatocarcinogenesis. J Clin Invest 2012;122:2884–2897
32. Yang J, Chen S, Huang L, Michalopoulos GK, Liu Y. Sustained expression of naked plasmid DNA encoding hepatocyte growth factor in mice promotes liver and overall body growth. Hepatology 2001;33:848–859
33. Guo J, Fang W, Sun L, et al. Reduced miR-200b and miR-200c expression contributes to abnormal hepatic lipid accumulation by stimulating JUN expression and activating the transcription of srebp1. Oncotarget 2016;7:36207–36219
34. Al-Obaide MA, Alobydi H, Abdelsalam AG, Zhang R, Srivenugopal KS. Multifaceted roles of 5′-regulatory region of the cancer associated gene B4GALT1 and its comparison with the gene family. Int J Oncol 2015;47:1393–1404
35. Hou WF, Zhang SP, Davidkova G, Nichols RA, Weiss B. Effect of antisense oligodeoxynucleotides directed to individual calmodulin gene transcripts on the proliferation and differentiation of PC12 cells. Antisense Nucleic Acid Drug Dev 1998; 8:295–308
36. Oh KJ, Han HS, Kim MJ, Koo SH. CREB and FoxO1: two transcription factors for the regulation of hepatic gluconeogenesis. BMB Rep 2013;46:567–574
37. O-Sullivan I, Zhang W, Wasserman DH, et al. FoxO1 integrates direct and indirect effects of insulin on hepatic glucose production and glucose utilization. Nat Commun 2015;6:7079
38. Jang H, Lee GY, Selby CP, et al. SREBP1c-CRY1 signalling represses hepatic glucose production by promoting FOXO1 degradation during refeeding. Nat Commun 2016;7:12180
39. Titchenell PM, Chu Q, Monks BR, Birnbaum MJ. Hepatic insulin signalling is dispensable for suppression of glucose output by insulin in vivo. Nat Commun 2015; 6:7078
40. Qu S, Altomonte J, Perdomo G, et al. Aberrant forkhead box O1 function is associated with impaired hepatic metabolism. Endocrinology 2006;147:5641–5652
41. Wang Y, Viscarra J, Kim SJ, Sul HS. Transcriptional regulation of hepatic lipogenesis. Nat Rev Mol Cell Biol 2015;16:678–689
42. Rodríguez A, Catalán V, Gómez-Ambrosi J, et al. Insulin- and leptin-mediated control of aquaglyceroporins in human adipocytes and hepatocytes is mediated via the PI3K/Akt/mTOR signaling cascade. J Clin Endocrinol Metab 2011;96:E586–E597
43. Berchtold MW, Villalobo A. The many faces of calmodulin in cell proliferation, programmed cell death, autophagy, and cancer. Biochim Biophys Acta 2014;1843: 398–435
44. Li RJ, Xu J, Fu C, et al. Regulation of mTORC1 by lysosomal calcium and calmodulin. eLife 2016;5: e19360
45. Meex RCR, Watt MJ. Hepatokines: linking nonalcoholic fatty liver disease and insulin resistance. Nat Rev Endocrinol 2017;13:509–520
46. Roy R, Durie D, Li H, et al. hnRNPA1 couples nuclear export and translation of specific mRNAs downstream of FGF-2/S6K2 signalling. Nucleic Acids Res 2014;42: 12483–12497
47. Jo OD, Martin J, Bernath A, Masri J, Lichtenstein A, Gera J. Heterogeneous nuclear ribonucleoprotein A1 regulates cyclin D1 and c-myc internal ribosome entry site function through Akt signaling. J Biol Chem 2008;283:23274–23287
48. Siculella L, Tocci R, Rochira A, Testini M, Gnoni A, Damiano F. Lipid accumulation stimulates the cap-independent translation of SREBP-1a mRNA by promoting hnRNP A1 binding to its 5′-UTR in a cellular model of hepatic steatosis. Biochim Biophys Acta 2016;1861:471–481
49. Luan W, Wang Y, Chen X, et al. PKM2 promotes glucose metabolism and cell growth in gliomas through a mechanism involving a let-7a/c-Myc/hnRNPA1 feedback loop. Oncotarget 2015;6:13006–13018
50. David CJ, Chen M, Assanah M, Canoll P, Manley JL. HnRNP proteins controlled by c-Myc deregulate pyruvate kinase mRNA splicing in cancer. Nature 2010;463: 364–368
51. Doumatey AP, Xu H, Huang H, et al. Global gene expression profiling in omental adipose tissue of morbidly obese diabetic African Americans. J Endocrinol Metab 2015;5:199–210
52. Kaminska D, Hämäläinen M, Cederberg H, et al. Adipose tissue INSR splicing in humans associates with fasting insulin level and is regulated by weight loss. Diabetologia 2014;57:347–351
53. Amamoto T, Kumai T, Nakaya S, Matsumoto N, Tsuzuki Y, Kobayashi S. The elucidation of the mechanism of weight gain and glucose tolerance abnormalities induced by chlorpromazine. J Pharmacol Sci 2006;102:213–219